Hindawi
International Journal of Aerospace Engineering
Volume 2021, Article ID 6656422, 16 pages
https://doi.org/10.1155/2021/6656422

Research Article

Typical Fault Estimation and Dynamic Analysis of a Leader-Follower Unmanned Aerial Vehicle Formation

Jian Shen,[1] **Qingyu Zhu**,[2] **Xiaoguang Wang**,[3] **and Pengyun Chen**[1]

[1]*College of Mechatronics Engineering, North University of China, Tai Yuan 030051, China*
[2]*AVIC China Aero-Polytechnology Establishment, Beijing 100028, China*
[3]*Department of Smart Ammunition, Norinco Group Aviation Ammunition Research Institute, Harbin 150030, China*

Correspondence should be addressed to Jian Shen; shenjian@nuc.edu.cn

Received 7 October 2020; Revised 3 March 2021; Accepted 9 March 2021; Published 26 March 2021

Academic Editor: Giovanni Palmerini

In this paper, the typical fault estimation and dynamic analysis are presented for a leader-follower unmanned aerial vehicle (UAV) formation system with external disturbances. Firstly, a dynamic model with proportional navigation guidance (PNG) control of the UAV formation is built. Then, an intermediate observer design method is adopted to estimate the system states and faults simultaneously. Based on the graph theory, the topology relationship between each node in the UAV formation has been also analyzed. The estimator and the system error have been created. Moreover, the typical faults, including the components failure, airframe damage, communication failure, formation collision, and environmental impact, are also discussed for the UAV system. Based on the fault-tolerant strategy, five familiar fault models are proposed from the perspectives of fault estimation, dynamical disturbances, and formation cooperative control. With an analysis of the results of states and faults estimation, the actuator faults can be estimated precisely with component failure and wind disturbances. Furthermore, the basic dynamic characteristics of the UAV formation are discussed. Besides, a comparison of two cases related to the wind disturbance has been accomplished to verify the performance of the fault estimator and controller. The results illustrate the credibility and applicability of the fault estimation and dynamic control strategies for the UAV system which are proposed in this paper. Finally, an extension about the UAV formation prognostic health management system is expounded from the point of view of the fault-tolerant control, dynamic modeling, and multifault estimation.

1. Introduction

In most developed fields of unmanned aerial vehicle (UAV), formation flight is one of the most important techs in swarm cooperative work. Multiple UAVs in a formation are more efficient than a single one during the process of mission completion. The swarm cooperative flight technology has been paid a lot of attention in the UAV field. However, it just starts, and there are many significant problems needed to be solved. For example, assuming that the formation configuration is stable, one crucial question is how to maintain the reliability and stability of the UAV system. To make the UAV formation flying safer, fault diagnosis and fault-tolerant control will be the key solutions. When faults appear during the formation flight, they should be detected, localized, and corrected in a short time. Otherwise, the mission will fail. With the help of accurate and in-time fault diagnosis and reliable fault-tolerant control, the formation will be reconfigured, and communication between each other will be optimized. As a result, the UAV formation will fly in a safe and stable status. There are many different kinds of faults that arose and coupled in real flight. According to the different degrees of faults, they can be divided into an intermittent fault, sudden fault, and slow fault. If classified by different fault parts, they include the actuators, sensors, and communication failures which may cause the whole formation to work in chaos.

Due to the complex coupled relationships between different stages in formation, the fault diagnosis will be affected by parameter perturbation, external disturbance, and noses. The formation controller has no ideal robustness performance, and the control accuracy declines [1]. In the fault diagnosis field, an observer-based method is usually used. In the

process of observer design, disturbance decoupling should be considered carefully. Consequently, the uncertainties in fault diagnosis can be eliminated, and the formation control will be more robust. Separating the disturbances and faults helps fault diagnosis efficiency and reduces the rate of false fault judgment.

In engineering applications, there are several typical fault diagnosis methods for UAV formation, for instance, distributed fault detection, sliding mode observer, robust unknown input observer, fuzzy sliding mode observer, and neural network. In these methods, the observer-based is one of the most used for linear systems with perturbations [2–4] and nonlinear systems [5]. The thought of the observer-based fault diagnosis method is using the measurable input and output value of the UAV formation system to design the system state observer and measure the status. With the residual signal observation of the estimate and the actual value, the approximation of system fault can be estimated, and fault diagnosis will be accomplished. For the observer-based fault diagnosis method appliance in the UAV field, Negash illustrated a bank of unknown input observer- (UIO-) based distributed fault detection scheme to detect and identify the compromised UAV in the formation. A rule based on the residuals generated using the bank of UIO has been used to detect attacks. Moreover, an algorithm was developed to remove the faulty UAV from the network once an attack has been detected and the compromised UAV isolated while maintaining the formation flight with a missing UAV node. A numerical case study has demonstrated that the residual generated at the monitoring node UAV can successfully detect and isolate the cyberattack. And the faulty UAV removal algorithm has been shown to effectively remove the compromised UAV to maintain the formation accordingly [6]. Reference [7] introduced a sliding mode observer which is designed to reconstruct the actuator faults and then eliminate the influence of the actuator faults in the UAV formation fault-tolerant control. Simulation results verified that the active fault diagnosis and fault-tolerant control scheme proposed for the UAV formation system with actuator faults were effective. In [8], an UIO-based scheme was used for icing detection in overactuated unmanned aerial vehicles. Decision algorithms had been proposed to correctly identify possibly unexpected effects in the system dynamics. Moreover, the icing accommodation task was addressed, using a fault-tolerant control allocation scheme and exploiting input redundancy in the case of control surface failures, or by using an automated deicing subsystem in the case of ice accretion on airfoils. Rotondo et al. proposed a discrete-time linear parameter varying (LPV) UIO for the diagnosis of actuator faults and ice accretion in the UAV system. The proposed approach, which was suited for an implementation onboard, exploited a complete 6-degrees of THE freedom (DOF) UAV model, which included the coupled longitudinal/lateral dynamics and the impact of icing. The LPV formulation had the advantage of allowing the icing diagnosis scheme to be consistent with a wide range of operating conditions. The developed theory was supported by simulations illustrating the diagnosis of actuator faults and icing in a small UAV. The obtained results validate the effectiveness of the proposed approach [9]. Reference [10] stated that a new online detection strategy was developed to detect faults in sensors and actuators of the UAV systems. In this design, the weighting parameters of the neural network (NN) were updated by using the extended Kalman filter (EKF). Online weighting parameter adaptation helped to detect abrupt, intermittent, and incipient faults accurately. There had been applied the proposed fault detection system to a nonlinear dynamic model of the WVU YF-22 unmanned aircraft for its evaluation. The simulation results show that the new method has better performance in comparison with conventional recurrent neural network-based fault detection strategies [10]. A 3D leader–follower formation control problem was discussed in [11]. A novel control law and an adaptive disturbance observer have been explored for the swarms of fixed-wing UAVs with motion constraints and disturbances. The simulation results showed that the proposed method was effective whether there were disturbances existing. In [12], a novel distributed sliding mode control law has been investigated for the leader-follower UAV formation. Numerical simulations verified that the adjustable range of the followers' linear velocity was not required to be larger than that of the leaders, which was of significance in the leader-follower formation flight for a large scale of UAVs.

However, in the traditional observer-based fault diagnosis method, the observer matching conditions must be satisfied [13]. This goal usually could not be meet in real engineering applications. Under the condition that the system satisfies the strict positive realness conditions, in [14, 15], a self-adaptive fault estimation method was stated. With a comparison of the observer matching conditions, the strict positive realness conditions were more conservative. To solve these problems, an intermediate observer-based method was presented in [16]. An intermediate variable was built, and the fault estimation observer was designed. The estimated value of the built intermediate variable was used to calculate the fault value. The most advantage was that the observer matching conditions and the strict positive realness conditions would not be needed to be satisfied for the systems. It was desirable for the fault estimation in the UAV formation system. In [17], the author adopted this kind of intermediate observer into a network of dynamical systems with external disturbances. A distributed intermediate estimator was constructed for each node based on local output measurements. Except for the built intermediate fault estimator, the interconnected relationship between UAVs should be considered. Additionally, the dimension of the linear matrix inequality (LMI) would increase with the growth of UAV number. These problems ought to be thought seriously when designing the UAV formation's fault estimator.

In [13], a new intermediate estimator was introduced to estimate the fault in a multiagent system. It could be used in a system which could not meet the observer matching conditions. Also, in the estimation of intermediate variables, the feedback effect of the output error was taken into account. In consequence, the estimation performance could be improved. Finally, the dimension of linear matrix inequality (LMI) will not enhance with the increase of UAV number.

In this paper, the typical fault modeling and simulation for a leader-follower UAV formation system, like the components failure, airframe damage, communication failure, formation collision, and environmental impact, will be the main focuses through the research process of fault estimation and dynamic analysis. A kinematic model of the leader and follower UAV is built, and the relative relationship will be maintained with the PNG control method in Section 2. To estimate the system states and faults, an intermediate observer design method is adopted in Section 3. The communication topology between each node in the UAV formation is built based on the graph theory. The estimator and estimation error model are also shown in this part. Furthermore, the typical faults are also discussed and modeled in Section 4. Then, the fault estimation and the dynamic analysis will be shown in the simulation and discussion part. With the analysis of the results, the future research extensions about the UAV formation fault diagnosis and cooperative control are concluded in the final part.

2. Dynamic Model of the UAV Formation

During the flight of the UAV formation, each member has a relative relationship of motion. According to different formation configurations, the definitions of the coordinate systems are not the same. In this section, a leader-follower scheme has been adopted to set up the formation [1]. Assuming that n UAVs are flying in the two-dimensional plane, considering the kinematics and dynamics of the leader and follower, the relative position relationship between them is shown in Figure 1.

In Figure 1, L is the leader, and F_i is the ith follower in the UAV system. The velocities for leader and follower are V_L and V_{F_i}, respectively. $X_L$and Y_L are the coordinates of the inertial system of leader, respectively. X_{Fi} and Y_{Fi} are the coordinates of the inertial system of follower, respectively. ψ_L and ψ_{Fi} are the pitch angles of leader and follower. R_L and R_{Fi} are the radius vectors of leader and follower.

According to the relative position relationship shown in Figure 1, the kinematic equations of leader and follower can be illustrated as [18]

$$\begin{cases} \dot{X}_L = V_L \cos \psi_L \\ \dot{Y}_L = V_L \sin \psi_L \\ \dot{\psi}_L = \omega_L \\ \dot{X}_{F_i} = V_{F_i} \cos \psi_{F_i} \\ \dot{Y}_{F_i} = V_{F_i} \sin \psi_{F_i} \\ \dot{\psi}_{F_i} = \omega_{F_i} \\ e_{F_i} = \begin{bmatrix} X_L - X_{F_i} \\ Y_L - Y_{F_i} \end{bmatrix} \end{cases} \quad i = 1, 2, \cdots, n, \tag{1}$$

where ω_L and ω_{Fi} are the pitch angle velocities of leader and follower. e_{F_i} is the leader-follower relative distance error.

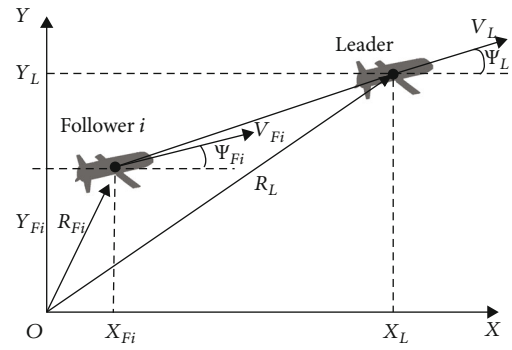

Figure 1: Relative position relationship between leader and follower in the UAV formation.

Under the inertial system, the second-order derivative of e_{F_i} is the function of control input and the control inputs which can be shown as

$$\begin{cases} \ddot{e}_{F_i} = f(u_{Fi}), \\ u_L = N{V_L}^2 \sin(\psi_L)/R_L, \\ u_{Fi} = N{V_{Fi}}^2 \sin(\psi_{Fi})/R_{Fi}, \end{cases} \tag{2}$$

where u_L and u_{Fi} are the UAV formation system control inputs for leader and follower which are based on the proportional navigation guidance (PNG) method. N is the scale factor of PNG.

A linearized and topology distributed UAV formation model is shown as

$$\begin{cases} \dot{x}_i(t) = Ax_i(t) + Bu_i(t) + Ff_i(t) + Ed_i(t) \\ y_i(t) = Cx_i(t), \end{cases}, \tag{3}$$

where $x_i(t) = [X_i\ Y_i\ \omega_i\ \psi_i]^T$ contains the states of the ith node in the UAV formation (including leader). The system control output is $y_i(t)$. $f_i(t)$ denotes the fault of UAV. $d_i(t)$ represents the system disturbance. A, B, C, E, and F are the coefficient matrixes.

2.1. Intermediate Observer-Based Fault Estimator of the UAV Formation. In the process of intermediate observer design, the centralized and distributed output estimation errors are considered at the same time. For the UAV formation with oriented topology connection, a low order LMI can be solved to calculate the observer gain matrix which is based on Schur matrix decomposition theory. The dimension of LMI is the same as the one which is related to the solved LMI dimension in fault estimation for a single UAV. As a result, for the intermediate fault estimator in [13], the amount of computation will not increase even more UAVs joined in the formation. In addition, for the UAV formation with unoriented topology, due to the symmetry of the Laplacian matrix, the strict positive realness conditions are less conservative.

2.1.1. Graph Theory. If there are n UAVs connected in one formation, the connection relationship based on graph theory can be proposed as

$$\varsigma = (\nu, \varepsilon, \Gamma), \tag{4}$$

where $\nu = \{\nu_1, \nu_2, \cdots, \nu_n\}$ represents the member set of the UAV formation, and the ith node is $\nu_i (i = 1, 2, \cdots, n)$. The edge set is $\varepsilon = \{(\nu_i, \nu_j): \nu_i, \nu_j \in \nu\} \subset \nu \times \nu$. The adjacency matrix of graphs is $\Gamma = [\Gamma_{ij}] \in \mathbf{R}^{n \times n}$, which can be shown as

$$\Gamma_{ij} = \begin{cases} 0, & i = j \\ 1, & (\nu_i, \nu_j) \in \varepsilon \\ 0, & \text{other} \end{cases}. \tag{5}$$

Assuming that $\nu_i$and ν_j are two connected nodes in the UAV formation, for one formation with unoriented topology connection, $(\nu_i, \nu_j) \in \varepsilon$ and $(\nu_j, \nu_i) \in \varepsilon$ are all established. But for the one with oriented topology connection, $(\nu_i, \nu_j) \in \varepsilon$ or $(\nu_j, \nu_i) \in \varepsilon$ is founded.

The symmetric Laplacian matrix $L = [L_{ij}] \in \mathbf{R}^{n \times n}$ of the graph is

$$L_{ij} = \begin{cases} \sum_{j=1}^{N} \Gamma_{ij}, i = j \\ -\Gamma_{ij}, i \neq j \end{cases}. \tag{6}$$

As mentioned above, the observer matching conditions or the strict positive realness conditions must be satisfied for the system fault estimator design. It means that CF in (3) is a matrix with a full rank column. But for the intermediate observer-based estimator, the above conditions are not needed to meet. The derivation process is shown in [13].

2.1.2. Intermediate Observer. The intermediate variable is defined as

$$\eta_i(t) = f_i(t) - Sx_i(t), \tag{7}$$

where S is a matrix which needed to be designed. The derivation of $\eta_i(t)$ is

$$\begin{aligned} \dot{\eta}_i(t) = \dot{f}_i(t) - S\dot{x}_i(t) = \dot{f}_i(t) - (SA + SFS)x_i(t) - SBu_i(t) \\ - SF\eta_i(t) - SEd_i(t). \end{aligned} \tag{8}$$

Combining (3) and (8), the intermediate estimator can be shown as

$$\begin{cases} \dot{\hat{x}}_i(t) = A\hat{x}_i(t) + Bu_i(t) + F\hat{f}_i(t) + \rho_1 K_1 \zeta_{1i}(t) + \rho_2 K_2 \zeta_{2i}(t), \\ \dot{\hat{\eta}}_i(t) = -SF\hat{\eta}_i(t) - (SA + SFS)\hat{x}_i(t) - SBu_i(t) + \rho_1 K_3 \zeta_{1i}(t) + \rho_2 K_4 \zeta_{2i}(t), \\ \hat{f}_i(t) = \hat{\eta}_i(t) + S\hat{x}_i(t), \end{cases} \tag{9}$$

where $\hat{x}_i(t)$ and $\hat{\eta}_i(t)$ are the estimations of the system states and the intermediate variable. $\hat{f}_i(t)$is the estimated value of faults. The centralized output estimation error and distributed output estimation error are $\zeta_{1i}(t)$ and $\zeta_{2i}(t)$. ρ_1 and ρ_2 are the weights of $\zeta_{1i}(t)$ and $\zeta_{2i}(t)$, respectively. K_1, K_2, K_3, and K_4 are the gain matrixes of the observer. ρ_1 and ρ_2 are all positive, and the sum of them equals one.

Figure 2: Component failure (e.g., actuator fault) in the UAV formation.

$\zeta_{1i}(t)$ and $\zeta_{2i}(t)$ can be defined as

$$\begin{cases} \zeta_{1i}(t) = y_i(t) - \hat{y}_i(t), \\ \zeta_{2i}(t) = \sum_{j=1}^{N} A_{ij} \left[(y_i(t) - \hat{y}_i(t)) - \left(y_j(t) - \hat{y}_j(t) \right) \right], \end{cases} \tag{10}$$

where $\hat{y}_i(t) = C\hat{x}_i(t)$ is the output estimation of the i'th node.

2.1.3. System Error. In order to evaluate the estimation errors, the sets of equality are adopted as

$$\begin{cases} \tilde{x}_i(t) = x_i(t) - \hat{x}_i(t), \\ \tilde{\eta}_i(t) = \eta_i(t) - \hat{\eta}_i(t), \\ \tilde{f}_i(t) = f_i(t) - \hat{f}_i(t). \end{cases} \tag{11}$$

The derivations of the estimation errors $\tilde{x}_i(t)$ and $\tilde{\eta}_i(t)$ are proposed as

$$\begin{cases} \dot{\tilde{x}}_i(t) = \dot{x}_i(t) - \dot{\hat{x}}_i(t) = A\tilde{x}_i(t) + F\tilde{f}_i(t) + Ed_i(t) - \rho_1 K_1 \zeta_{1i}(t) - \rho_2 K_2 \zeta_{2i}(t), \\ \dot{\tilde{\eta}}_i(t) = \dot{\eta}_i(t) - \dot{\hat{\eta}}_i(t) = -SF\tilde{\eta}_i(t) - (SA + SFS)\tilde{x}_i(t) - SEd_i(t) + \dot{f}_i(t) - \rho_1 K_3 \zeta_{1i}(t) - \rho_2 K_4 \zeta_{2i}(t). \end{cases} \tag{12}$$

In [16, 17], the designed matrix S is

$$S = \mu F^T. \tag{13}$$

If the value of the empirically selected parameter μ is larger, the convergence rate is faster, and the overshoot is bigger [19]. With derivation, the estimation errors of the UAV formation can be illustrated as

$$\begin{cases} \dot{\xi}(t) = I_N \otimes \left(A_1 - \rho_1 \bar{K}_1 C_1 \right) \xi(t) - L \otimes \rho_2 \bar{K}_2 C_1 \xi(t) + I_N \otimes E_1 \omega(t), \\ Y(t) = I_N \otimes \bar{C} \xi(t), \end{cases} \tag{14}$$

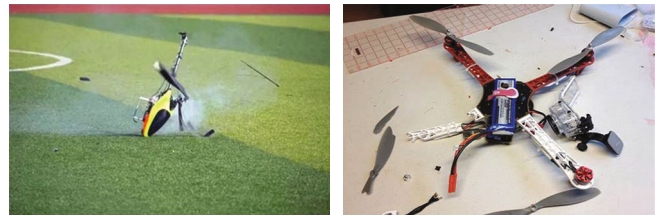

Figure 3: Airframe damage of UAV.

where

$$\begin{aligned}\xi(t) &= \left[\xi_1^T(t), \xi_2^T(t), \cdots, \xi_N^T(t)\right],\\ \omega(t) &= \left[\omega_1^T(t), \omega_2^T(t), \cdots, \omega_N^T(t)\right],\\ Y(t) &= \left[Y_1^T(t), Y_2^T(t), \cdots, Y_N^T(t)\right].\end{aligned} \tag{15}$$

And the matrixes in (14) are

$$\begin{aligned}A_1 &= \begin{bmatrix} A+\mu FF^T & F \\ -\mu F^T\left(A+\mu FF^T\right) & -\mu F^T F \end{bmatrix},\\ E_1 &= \begin{bmatrix} E & O_{n\times nf} \\ -\mu F^T E & I_{nf} \end{bmatrix},\\ \bar{K}_1 &= \begin{bmatrix} K_1 \\ K_3 \end{bmatrix}, \bar{K}_2 = \begin{bmatrix} K_2 \\ K_4 \end{bmatrix},\\ C_1 &= \begin{bmatrix} C & O_{ny\times nf} \end{bmatrix}, \omega(t) = \begin{bmatrix} d_i(t) \\ \dot{f}_i(t) \end{bmatrix},\end{aligned} \tag{16}$$

where n, nf and ny are the dimensions of nodes number, faults, and outputs.

In [13], the different forms of (14) for the UAV formation with oriented and unoriented topology connection were also derived. Moreover, the stability of system error (14) was already proved in this reference. It will not be repeated here.

2.2. Typical Fault Models of the UAV Formation

2.2.1. Typical Fault Introduction. During the flight of the UAV formation, the vehicles may be affected by many factors, such as the actuator jam, airframe damage, communication failure, collisions, or environmental impact. These factors, regarded as the typical faults of the UAV formation, may occur at the same time, or one thing happening causes the other to happen. To maintain the safety and reliability of the UAV formation flight, a fault-tolerant health management system must be designed to handle these faults [20]. The descriptions and responses of the typical faults are illustrated as follows.

(1) The Component Failure of UAV. Failures of the onboard actuators, sensors, control systems, flight computers, power systems, and other components are collectively referred to the component level failure [21–24]. An example of the actuator fault in the UAV formation is shown in Figure 2.

Figure 4: Information flow failure in the UAV formation.

For component failures of the UAV formation, the health management system can monitor fault signals online in real-time and reduce the impact of measurement deviation and signal drift on system performance through algorithm optimization and other measures [25].

(2) Airframe Damage. Failures of the UAV formation, such as collision with neighboring members or obstacles, may cause damage to the airframe. These failures, as shown in Figure 3, belong to the components level faults. The impact of components or UAV body damage on formation performance is determined by the effectiveness of the health management system [26].

When the components are damaged, the health management system provides the control system with a control scheme adapted to the current situation through online identification and adaptive technology [27].

(3) Communication Failure. Temporary or permanent loss of communication signals between connected members in Figure 4 is caused by interference or communication device failure [28].

When information flow failure occurs in formation, the health management system should make up for the lost information in time to accomplish the tasks [29].

(4) Formation Collision. When UAV deviates from the planned track or the expected motion state, it is considered that the formation is abnormal. This increases the risk of collision with obstacles or neighboring aircrafts [30, 31] like what is shown in Figure 5.

If the formation of UAVs is abnormal and colliding, the monitoring system quickly acquires abnormal information

Figure 5: Collision occurred in the UAV formation.

and notices each member. The health management system adopts control decision optimization to adjust the configuration of the formation and the relative movement relationship of nodes in real-time [32, 33].

(4) Environmental Impact. Severe weather (Figure 6) or environmental factors cause performance degradation or failure of the UAV communication system, control system, and actuator [34].

The health management system can monitor the characteristics and signals of the working environment and meteorological conditions and adjust the formation according to real-time feedback.

2.2.2. Modeling of the Typical Faults

(1) Actuator Failure (AF). Typical actuator failures include lock-in place, harder over fault, and floating. During the flight of the UAV formation, any member's normal control input $u_{\text{in}}(t)$ has been taken by a faulty control signal $\bar{u}_i(t)$ which is corresponding to the actuator failure [35]. If the actuator fault of UAV happens at time t_f, the control input in (3) can be shown as

$$u_i(t) = u_{\text{in}}(t) + \sigma_{Ai}[u_i(t) - u_{\text{in}}(t)]. \tag{17}$$

The unit step function σ_{Ai} is expressed as

$$\sigma_{Ai} = \begin{cases} 1, & t \geq t_f \\ 0, & t < t_f \end{cases}, \tag{18}$$

(2) UAV Component Damage (UCD). The damages of UAV's components will lead to the change of the formation dynamics. These faults can be regarded as disturbance $d_{Di}(t)$ which belongs to a finite norm $L_2[0, +\infty)$ [17]. $d_{Di}(t)$ can be proposed as [16]

$$\|d_{Di}(t)\| < L_g \|\hat{x}_i(t) - x_i(t)\|, \tag{19}$$

where L_g is the Lipschitz constant.

Figure 6: UAV formation fly in extreme weather.

(3) Communication Failure (COMF). Take the leader-follower formation model as an example, the leader moves independently under the requirements of the planned task. Other followers just go after the leader and receive the state information from the leader periodically. The information flow among the formation nodes constitutes a communication topology, and every node modulates its own state based on the information. Time delay always exists in the communication process which may causes collision during the maneuvering of formation. As a result, the feedback strategy must be adopted in the communication topology to maintain the stability of the UAV formation [36, 37].

The communication failures include transmitter, receiver, and transceiver failures [28]. If the transmitter fails on any node, it may not communicate with other nodes according to the information received from the linked UAVs. Once the failure happened on the receiver, the faulty node will broadcast its decision to others, and the leader will make a new decision on the assignment of the targets for the formation again. In order to make the formation task achievable, the node, which has a partial or complete communication failure, will leave the formation safely and heads to the ground station following a prescribed escape maneuver. Meanwhile, the transceiver of this faulty node must be shut

down immediately to prevent its influence on the reconfigured communication topology.

For the communication topology reconfiguration, UAV connected adjacency matrix and the Laplacian matrix need to be reset. Figure 4 shows a connected formation configuration. If there is no communication failure exists, the connection adjacency matrix and the Laplacian matrix are proposed as

$$\Gamma = \begin{bmatrix} 0 & 1 & 1 & 0 \\ 1 & 0 & 1 & 0 \\ 1 & 1 & 0 & 1 \\ 0 & 0 & 1 & 0 \end{bmatrix}, L = \begin{bmatrix} 2 & -1 & -1 & 0 \\ -1 & 2 & -1 & 0 \\ -1 & -1 & 3 & -1 \\ 0 & 0 & -1 & 1 \end{bmatrix}. \quad (20)$$

If follower 2 has communication failure, it leaves the formation, and follower 3 links to follower 1. The index of follower 3 changes to 2. The connection adjacency matrix and the Laplacian matrix are shown as

$$\Gamma_{\text{COMF}} = \begin{bmatrix} 0 & 1 & 0 \\ 1 & 0 & 1 \\ 0 & 1 & 0 \end{bmatrix}, L_{\text{COMF}} = \begin{bmatrix} 1 & -1 & 0 \\ -1 & 2 & -1 \\ 0 & -1 & 1 \end{bmatrix}. \quad (21)$$

(4) Collision Failure (COLF). With the need for configuration maintenance, every node in the formation ought to hold a safe distance from its neighbors. If UAVs are too close to each other, the collision may happen. And if the distance is very long, the time delay of communication may cause other failures [38].

According to the desired safe distance r_{desire} sent by the leader, a scheme of collision avoidance is shown in Figure 7. Every node will get a reward value from the leader depending on the distance to its neighbors. Members in the formation will adjust their states based on these reward values.

The reward value is defined as

$$\text{reward}_i = \begin{cases} -1, & r_{ij} < r_{\min} \\ (-1, 0), & rij_{\text{desire}\min} \\ 0, & r_{ij} = r_{\text{desire}} \\ (0, 1), & r_{\text{desire}} < r_{ij} \le r_{\max} \\ 1, & r_{ij} > r_{\max} \end{cases}, \quad (22)$$

where $r_{\min}$ and $r_{\max}$ are the minimum and maximum distance between two connected nodes, respectively. Once collisions occur during the flight, the leader must affirm that whether the collided nodes are still in the topology. If that is the case, these nodes quit the formation and fly back to the base station following the leaving strategy as same as the communication failure.

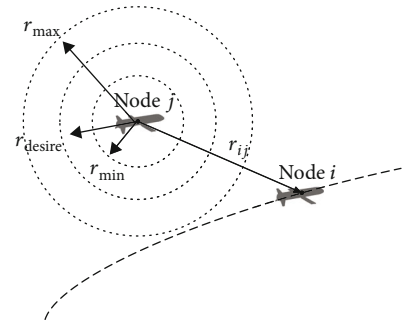

Figure 7: UAV formation collision avoidance scheme.

(5) Extreme Environment (EE). If the UAV formation flies in a real environment, such as desert, forest, valley, and ocean, many factors will affect the system's dynamic stability. For example, the low temperature in the polar region may freeze the wings of the actuator. Or if a UAV is struck by a thunderbolt, the internal communication equipment will be damaged, and the information cannot be transformed in time among the formation nodes. These baneful influences will lead to the failures of onboard actuators, sensors, and control systems. Except for the fault models that have been already mentioned in this section, a wind model is needed to be considered. The perturbation of wind is the main factor that causes flight failure though the design of the aircraft which is relatively perfect [39].

The influence of wind can be regarded as a part of the system disturbance $d_i(t)$. There are static and dynamic parts in a wind model. The speed of static wind can be proposed as

$$V_s(t) = V_{\text{const}} + V_a(t), \quad (23)$$

where V_{const} is the constant wind speed. $V_a(t)$ represents the time-varying part and can be illustrated as

$$V_a(t) = \begin{cases} 0 & , t \in [0, t_0] \cup (t_2, +\infty) \\ \dfrac{v_{s\max}(t - t_0)}{t_1 - t_0} & , t \in (t_0, t_1] \\ \dfrac{v_{s\max}(t - t_1)}{t_1 - t_2} & , t(t_1, t_2] \end{cases}, \quad (24)$$

where $V_{s\max}$ is the maximum value of the static wind. t_0, t_1, and t_2 are the time-varying wind speed increase, decrease, and disappear time.

The speed of the dynamic wind is complex and changes randomly over time. In engineering application, a simplified model has been set up as

$$V_d(t) = V_{d\max} r\text{and}(-1, 1) \sin 2\pi t + U(-\pi, \pi), \quad (25)$$

where $V_{d\max}$ is the maximum value of the dynamic wind. $U(-\pi, \pi)$ is a uniform distribution between $-\pi$ and π.

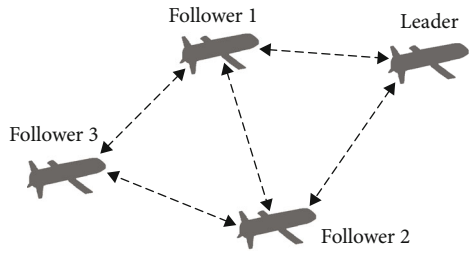

Figure 8: UAV formation both-way communication topology.

Table 1: Fault injected strategy.

Fault type	AF	UCD	EE
Leader	$f_L = \begin{cases} 0, t \in [0, 20) \\ 0.5\cos t, t \in [20, +\infty) \end{cases}$	$d_{\mathrm{DL}}(t)$	$d_{\mathrm{wL}}(t)$
Follower 1	$f_{F1} = \begin{cases} 0, t \in [0, 10) \\ 2.0, t \in [10, +\infty) \end{cases}$	$d_{\mathrm{DF1}}(t)$	$d_{\mathrm{wF1}}(t)$
Follower 2	No faults	$d_{\mathrm{DF2}}(t)$	$d_{\mathrm{wF1}}(t)$
Follower 3	$f_{F3} = \begin{cases} 0, t \in [0, 20) \\ -2e^{(-0.2t)}, t \in [20, +\infty) \end{cases}$	$d_{\mathrm{DF3}}(t)$	$d_{\mathrm{wF1}}(t)$

As mentioned above, the part which relates to the wind in system disturbance $d_i(t)$ can be shown as

$$d_{\mathrm{wi}}(t) = V_s(t) + V_d(t). \tag{26}$$

The total system disturbance can be illustrated as

$$d_i(t) = d_{\mathrm{Di}}(t) + d_{\mathrm{wi}}(t). \tag{27}$$

In this paper, the fault estimation will be the main contents which will be discussed in the next section. The basic models of typical faults are just derived in this section. Among these faults models mentioned above, COMF and COLF are relevant to the specific control model of the UAV formation. More simulation, verification and analysis about these two faults will be proposed in future research which will not be included in this paper.

3. Results and Discussion

A four-UAV formation is taken as an instance to analyze the dynamics and estimate different types of faults in this part. The both-way communication topology for the UAV formation is shown in Figure 8.

The connection adjacency matrix and the Laplacian matrix are shown as

$$\Gamma = \begin{bmatrix} 0 & 1 & 1 & 0 \\ 1 & 0 & 1 & 1 \\ 1 & 1 & 0 & 1 \\ 0 & 1 & 1 & 0 \end{bmatrix}, L = \begin{bmatrix} 2 & -1 & -1 & 0 \\ -1 & 3 & -1 & -1 \\ -1 & -1 & 3 & -1 \\ 0 & -1 & -1 & 2 \end{bmatrix}. \tag{28}$$

Table 2: Basic parameters.

Parameters	Unit	Value
Constant wind speed	m/s	V_{const} = rand $[-2, 2]$
Maximum static wind	m/s	$V_{s\,\max}$ = rand $[-5, 5]$
Maximum dynamic wind	m/s	$V_{d\,\max}$ = rand $[-15, 15]$
Wind speed increase time	s	$t_0 = 5$
Wind speed decrease time	s	$t_1 = 30$
Wind speed disappear time	s	$t_2 = 400$
Scale factor of PNG	—	$N = 3.0$
Estimation error weight	—	$\rho_1 = 0.5, \rho_2 = 0.5$
Observer parameter	—	$\mu = 1.2$

The coefficient matrixes in (3) are illustrated as

$$A = \begin{bmatrix} -3.5 & 7.0 & 0.0 & -3.5 \\ 3.5 & -7.0 & 3.5 & 0.0 \\ 0.0 & 3.5 & -3.5 & 0.0 \\ 3.5 & 0.0 & 3.5 & -3.5 \end{bmatrix}, C = \begin{bmatrix} 7.0 & 3.5 & 0.0 & -7.0 \\ 3.5 & 1.75 & 0.0 & 3.5 \\ 0.0 & 0.0 & 0.0 & 3.5 \end{bmatrix},$$
$$E = \begin{bmatrix} 3.5 \\ 3.5 \\ 3.5 \\ 3.5 \end{bmatrix}, F = \begin{bmatrix} 3.5 \\ -7.0 \\ 3.5 \\ 0.0 \end{bmatrix}, B = \begin{bmatrix} 0.0 \\ 3.5 \\ 3.5 \\ 3.5 \end{bmatrix}. \tag{29}$$

The gain matrixes for the intermediate observer, which are calculated by the LMI solver, can be shown as

$$K_1 = \begin{bmatrix} -11.9224 & 5.4709 & 19.5080 \\ 51.1084 & 38.2448 & -53.4466 \\ -17.5233 & 71.1116 & -29.4173 \\ -8.3095 & 20.6574 & 4.8709 \end{bmatrix},$$
$$K_2 = \begin{bmatrix} -1.4625 & 2.9249 & -5.8499 \\ 3.8633 & -7.7266 & 15.4532 \\ 0.3167 & -0.6337 & 1.2671 \\ -0.3082 & 0.6163 & -1.2326 \end{bmatrix},$$
$$K_3 = [\,73.3798 \quad -3.6015 \quad -50.7336\,],$$
$$K_4 = [\,4.7801 \quad -9.5604 \quad 19.1207\,]. \tag{30}$$

Fault simulation conditions are shown in Table 1.

The components' damages are assumed as a disturbance for the nodes in the formation. And formation UCD can be proposed as

$$d_{\mathrm{DL}}(t) = d_{\mathrm{DF}i}(t) = 0.5\mathrm{e}^{-3/\mathrm{t}}\mathrm{rand}[-2, 2], i = 1, 2, 3. \tag{31}$$

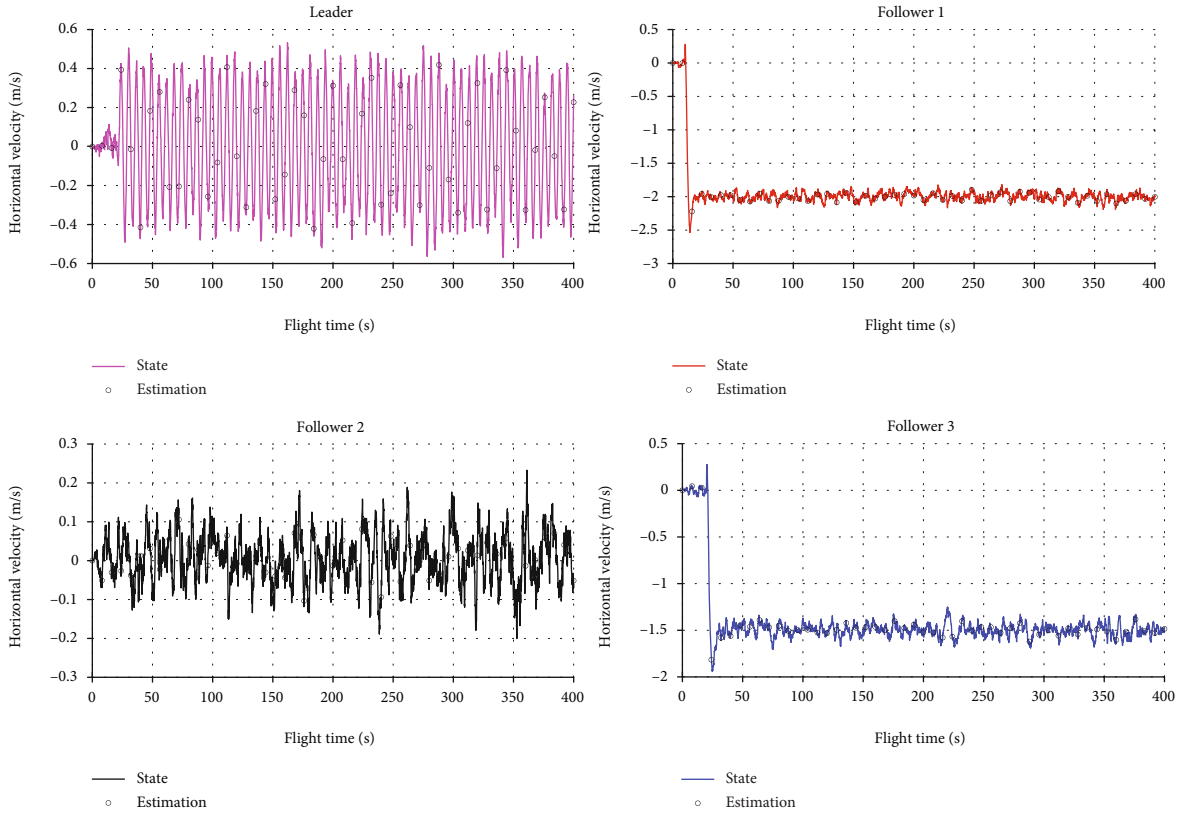

Figure 9: The system horizontal velocity and estimation.

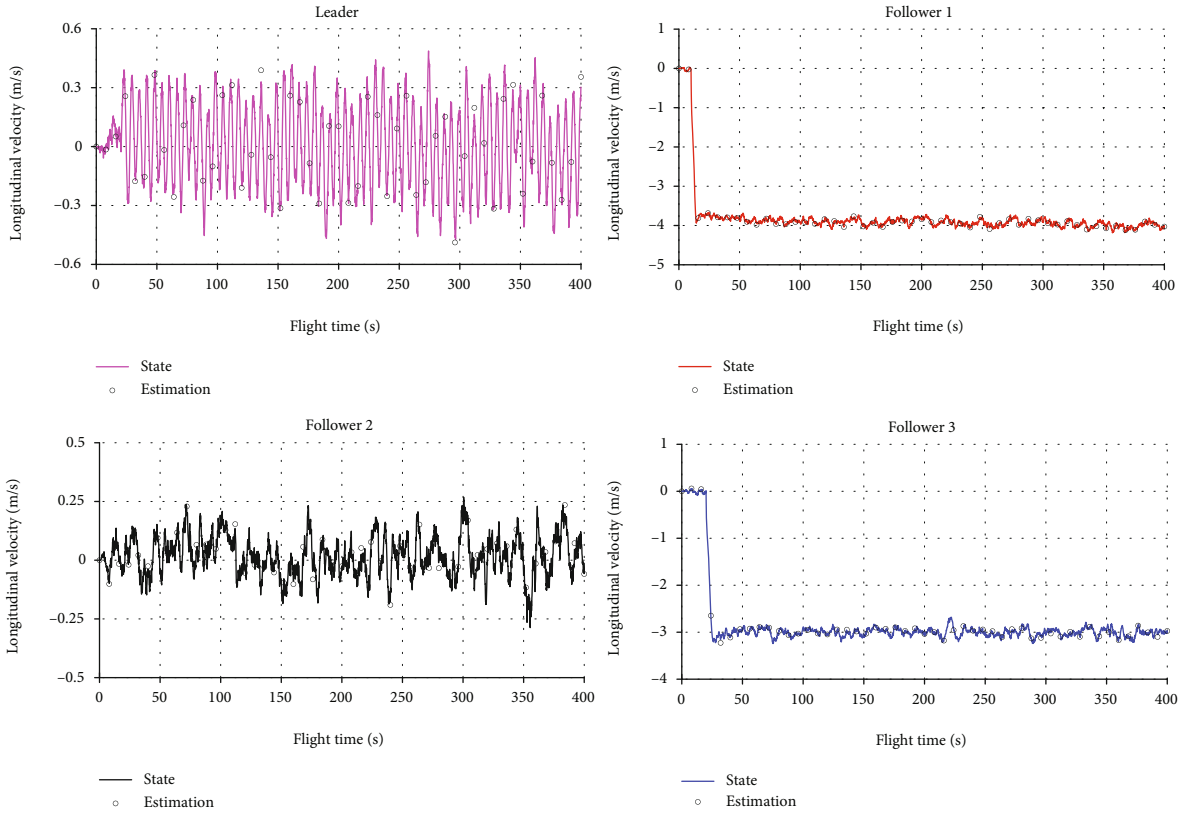

Figure 10: The system longitudinal velocity and estimation.

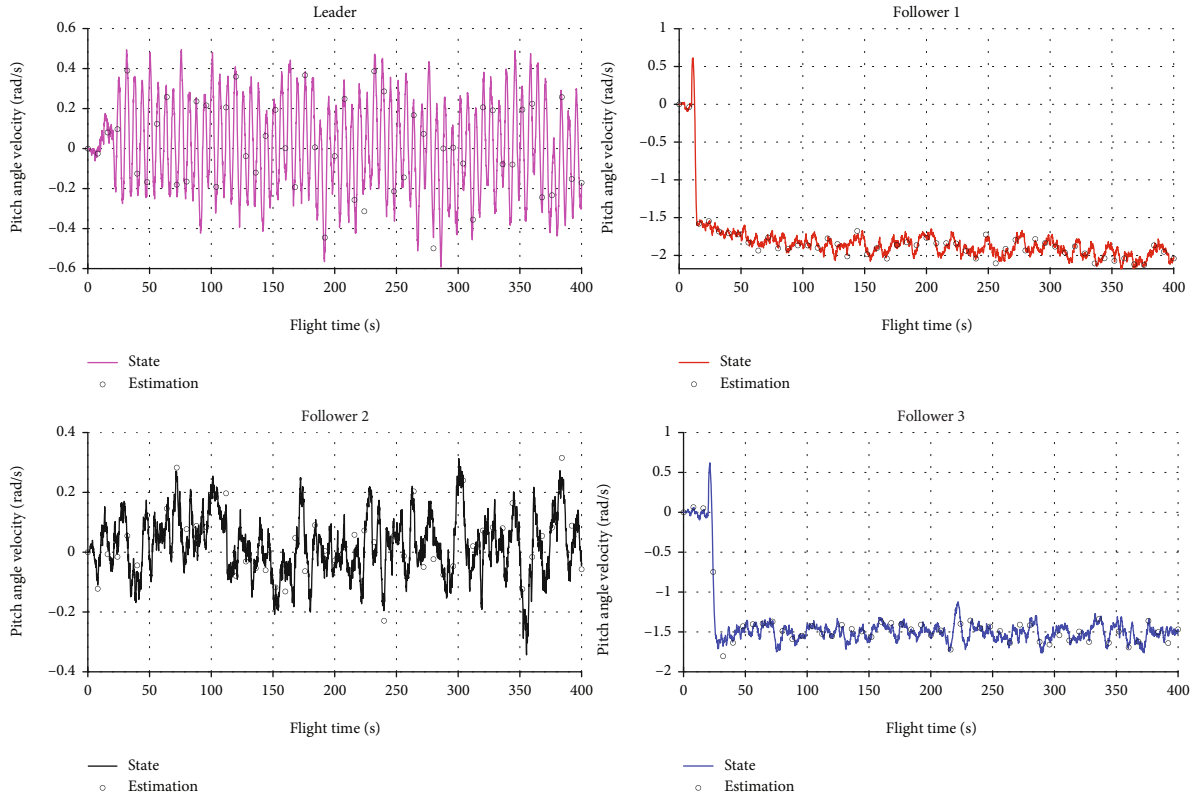

Figure 11: The system pitch angle velocity and estimation.

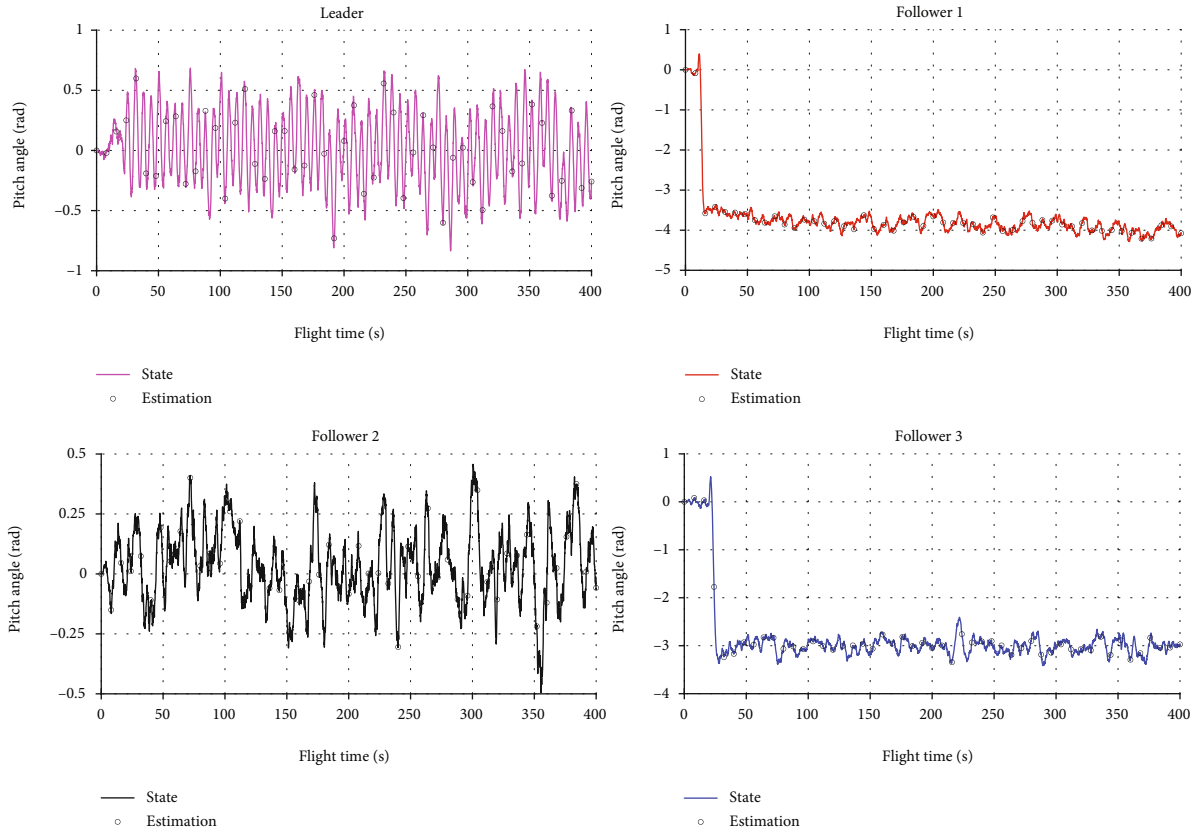

Figure 12: The system pitch angle and estimation.

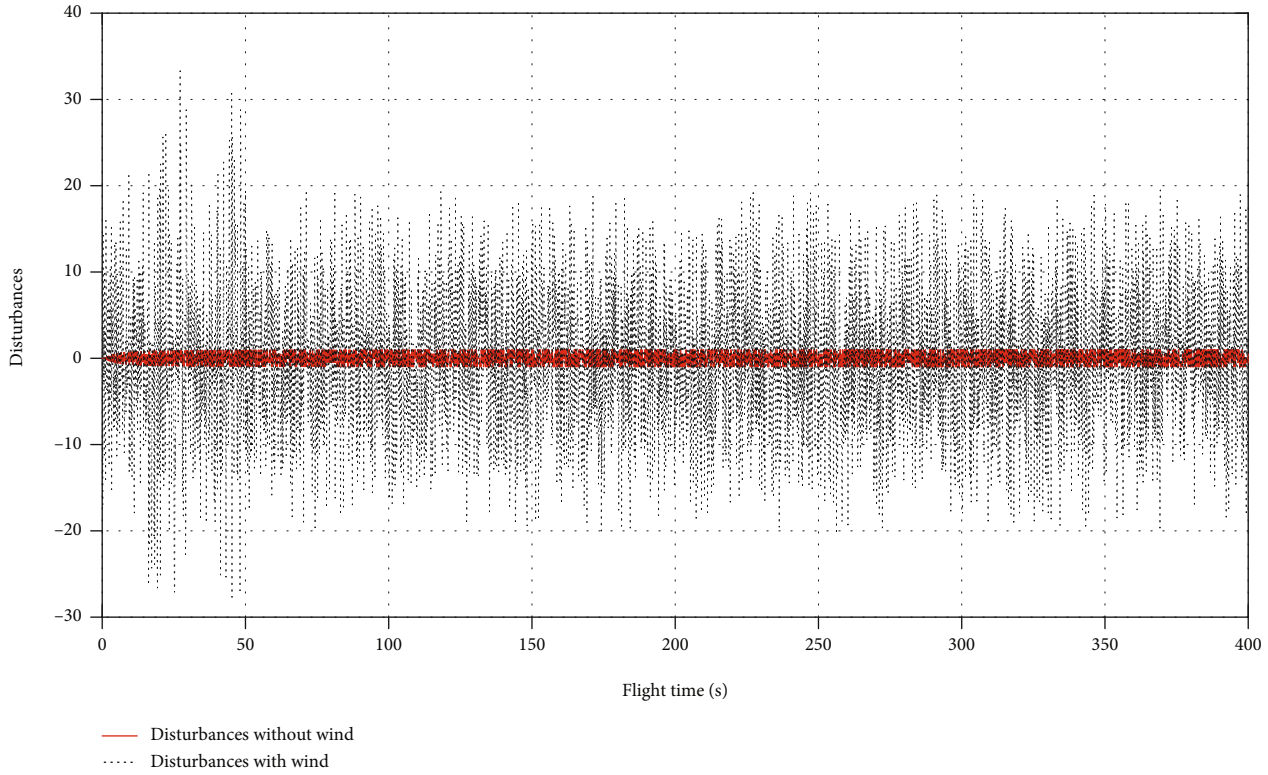

Figure 13: The disturbance comparison for the situations with or without wind.

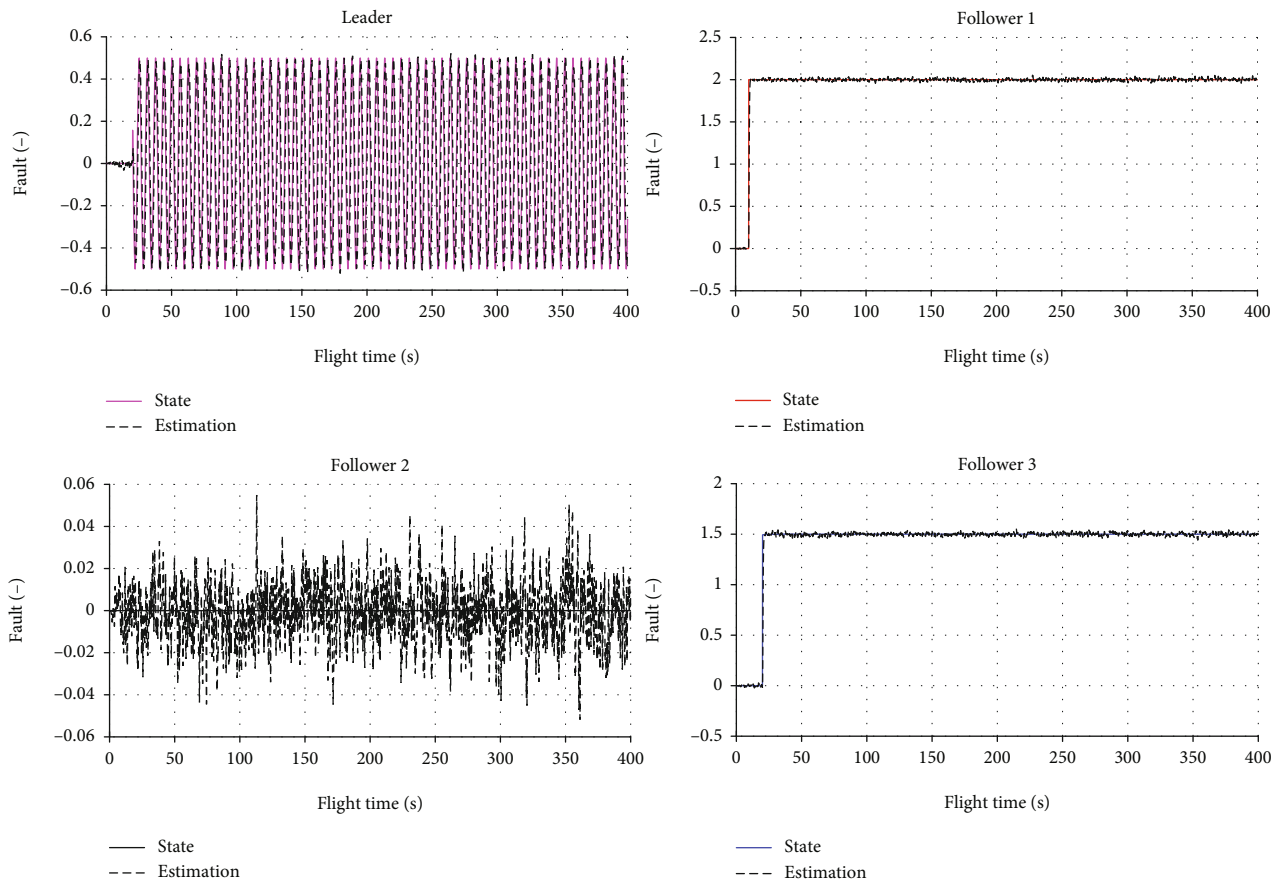

Figure 14: The faults and estimations for the UAV formation (without wind).

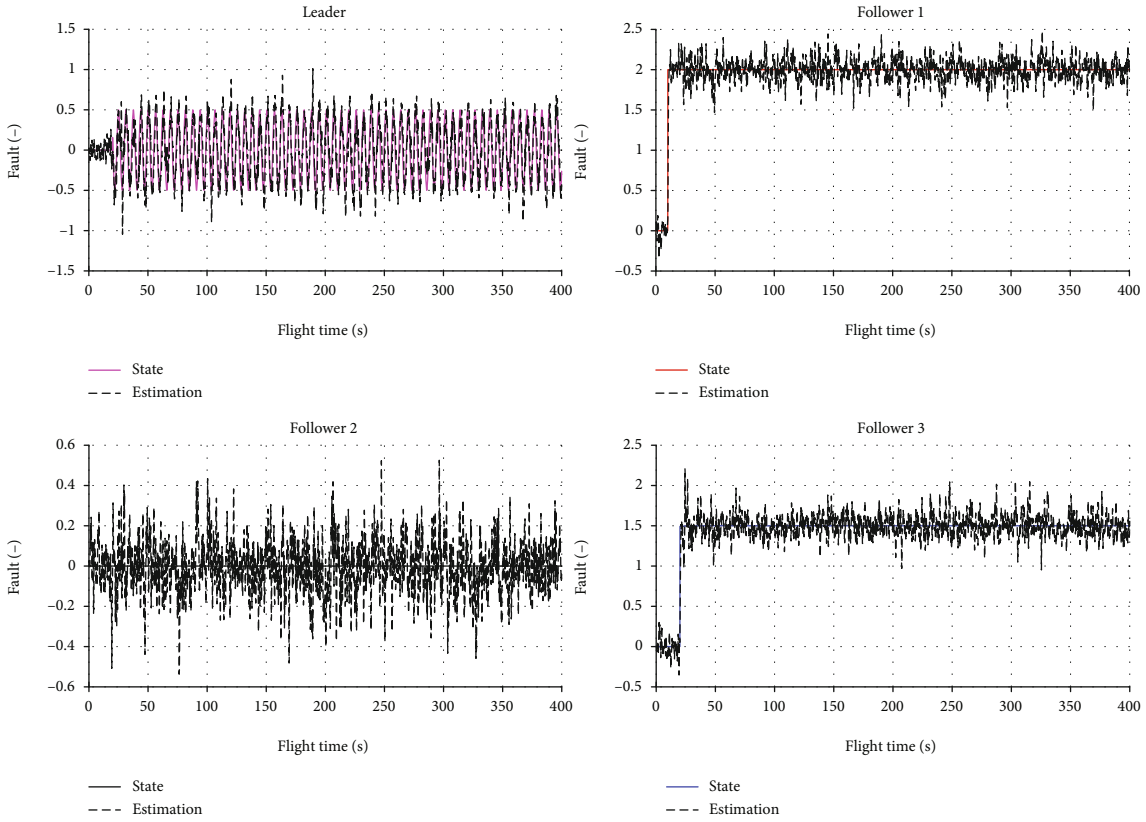

Figure 15: The faults and estimations for the UAV formation (with wind).

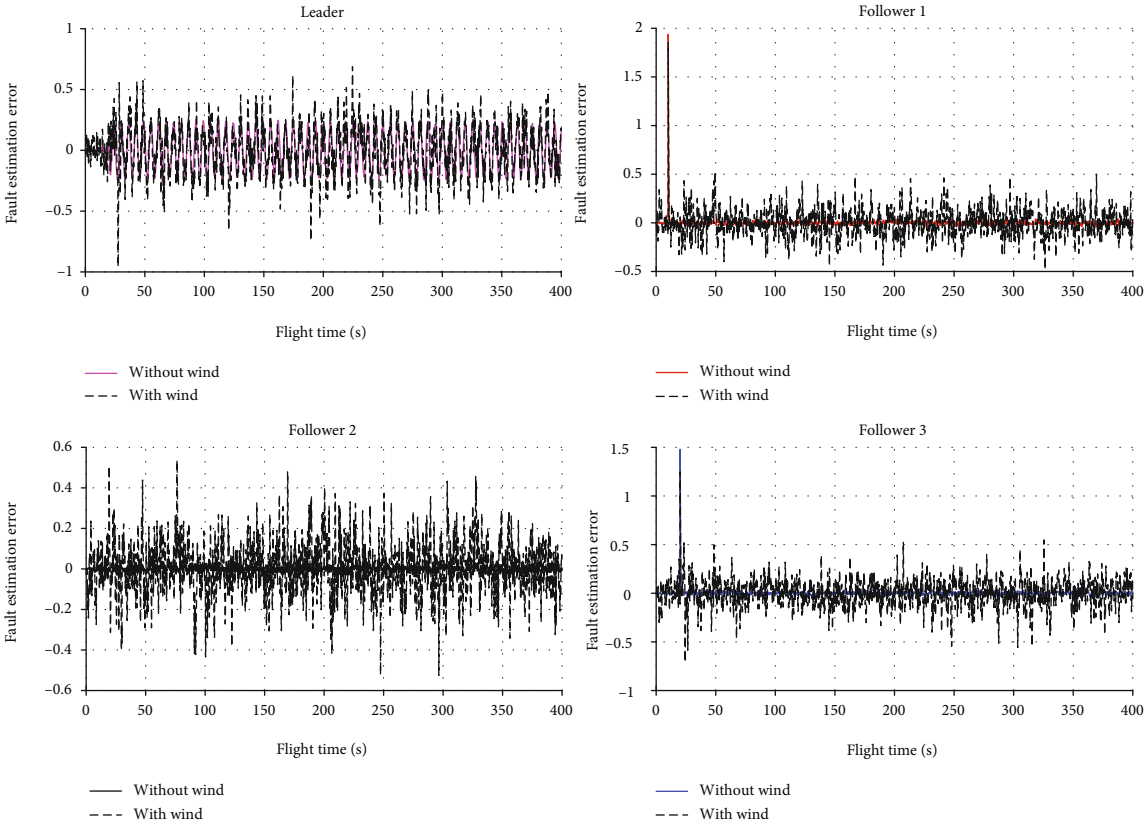

Figure 16: The fault estimation error comparison for the situations with or without wind.

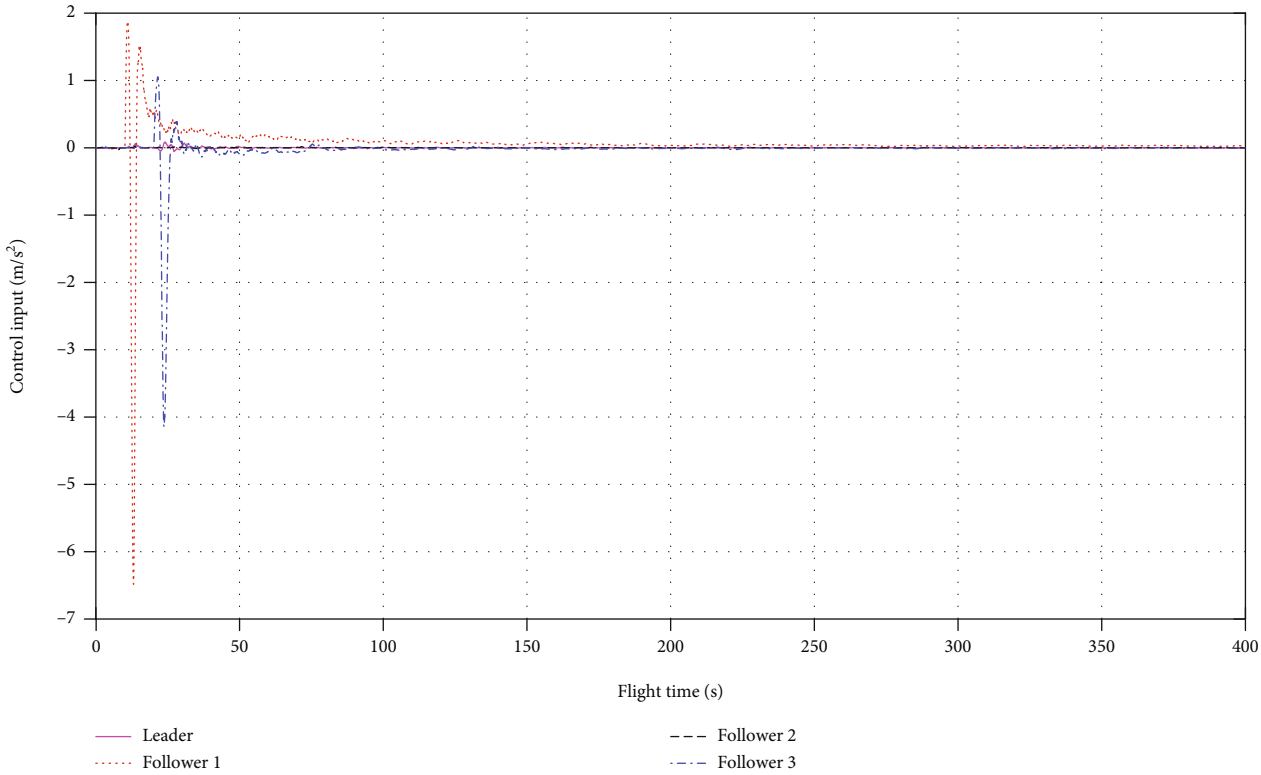

Figure 17: The control inputs for the UAV formation (without wind).

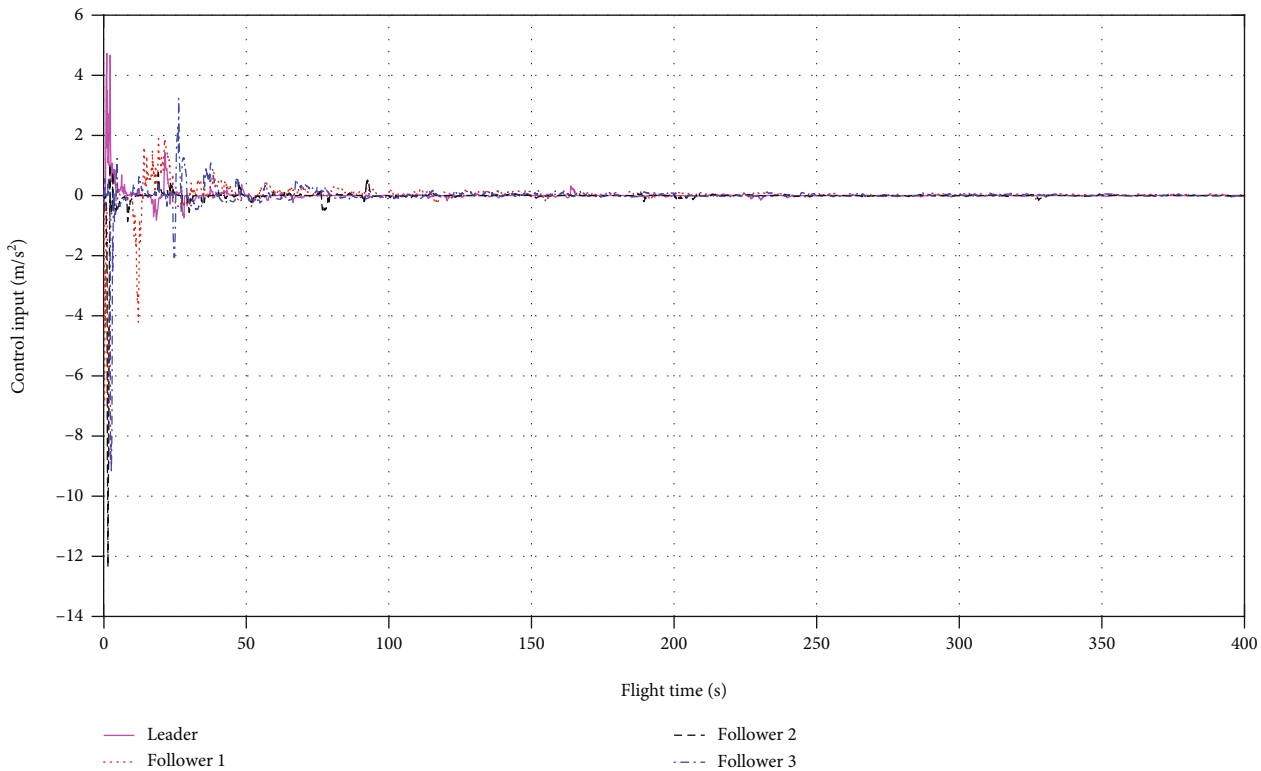

Figure 18: The control inputs for the UAV formation (with wind).

The wind disturbance model is

$$d_{\mathrm{wL}}(t) = d_{\mathrm{wF}i}(t) = V_s(t) + V_d(t), i = 1, 2, 3. \quad (32)$$

The basic parameters for the simulation are illustrated in Table 2.

Figures 9–12 (without wind disturbance) illustrate the system states and estimations for leaders and followers 1-3, respectively. As shown in these Figures, the states change dramatically after the faults appearing. For the leader, the actuator fault arises at $t = 20$ s, and the states change matches with the cosine curve basically. This fulfills the set of the AF fault model in Table 1. For the followers 1 and 3, the curves of states and estimation also meet the fault injected strategy. There is no AF fault that happened to follower 2, and the states and estimations results are just affected by the disturbances.

Figure 13 proposes the value comparison of disturbances for the EE fault situation (wind consideration). The amplitude ratio between with and without wind situations is up to a maximum of 60.99. In order to verify the influences of wind disturbances, the results of fault estimation are compared in Figures 14 and 15. In contrast to Figure 14, it shows obvious estimation errors increase in Figure 15. As the curves shown in Figure 16, take follower 1 as an example, the maximum average fault estimation errors of the system rise from 0.26% (without wind) to 0.51% (with wind).

From the comparison between Figures 17 and 18, it proposes that the wind disturbance aggravates the control inputs of the UAV formation. In Figure 17, the control inputs change gently, and the maximum amplitude is below 7 m/s^2. Due to the injected fault, leader and followers 1 and 3 need the PNG controller to be acting more to make the system stabler. Once the wind disturbance has been added into the system simulation, a rapid and high-frequency control signal emerged as what is shown in Figure 18. With the linear superposition of faults and disturbances, the maximum amplitude of control input exceeds 12 m/s^2, and it costs a longer time (nearly 150 second) for the controller convergence.

4. Conclusions

The fault estimation and dynamic analysis for the leader-follower UAV formation with typical faults were discussed in this paper. The kinematic model of leader and follower was built, and the PNG control model was adopted. Meanwhile, the linearized form of the system state equations was also represented in Section 2. To estimate the system states and faults, an intermediate observer-based estimator had been adopted for the UAV formation in Section 3. In this part, the connection relationship based on graph theory was proposed as the adjacency matrix of graphs and a symmetric Laplacian matrix. Next, it illustrated the intermediate estimator model and the estimation errors. In Section 4, the typical faults models were proposed with the basic concept, normal solution, and physical model. With the institution of the fault-tolerant strategy, five familiar faults models were discussed and derived according to the considerations of fault estimation, disturbances, control strategy, and dynamical analysis. According to the simulation results, the main typical fault estimation and dynamic characteristics of the UAV formation were accomplished. Moreover, it inspected the performance of the estimator and controller with two situations related to the wind disturbance. And the results showed that the fault estimation and dynamic control model were applicable for the UAV formation system.

In the real flight environment, faults and disturbance factors may arise at any time. As a result, the typical fault tolerance should be considered seriously in the fault-tolerant control design for the UAV formation. Additionally, for the sake of meeting the dynamic analysis needs, the model uncertainty, control output perturbation, time-lags effect, and nonlinear model ought to be thought during the modeling of the formation coordinated control strategy. Finally, multifault coupling, mixed estimation method, and multiestimators will be the important works in the UAV formation prognostic and health management field.

Data Availability

Hindawi research data policy request.

Conflicts of Interest

The authors declare that they have no conflicts of interest.

Acknowledgments

This work was supported by the National Natural Science Foundation of China [grant numbers 62003314, 51909245], Aeronautical Science Foundation of China [grant number 2019020U0002], Shanxi Province Applied Basic Research Project [grant numbers 201901D211244, 201801D221039], Scientific and Technological Innovation Programs of Higher Education Institutions in Shanxi [grant number 2019L0570], Youth Science and Technology Research Fund, and Science Foundation of North University of China [grant number XJJ201813].

References

[1] Y. Dong, *Research on Fault Diagnosis for UAVs formation Systems Based on Observer [M.S. thesis]*, Colg. Auto. Eng., Nanjing Univ., of Aero., Astro.,], 2018.

[2] X. Lin and X. Yao, "Improved disturbance-observer-based fault-tolerant control for the linear system subject to unknown actuator faults and multiple disturbances," *International Journal of Control*, vol. 93, no. 10, pp. 1–11, 2020.

[3] T. H. Lee, C. P. Lim, S. Nahavandi, and R. G. Roberts, "Observer-based H_∞ fault-tolerant control for linear systems with sensor and actuator faults," *IEEE Systems Journal*, vol. 13, no. 2, pp. 1981–1990, 2019.

[4] C. Liu, B. Jiang, and K. Zhang, "Sliding mode observer-based actuator fault detection for a class of linear uncertain systems," in *Proceedings of 2014 IEEE Chinese Guidance, Navigation and Control Conference*, pp. 230–234, Yantai, China, 2014.

[5] A. N. Hanafi, M. M. Seron, and J. A. De Doná, "Observer–based fault tolerant control for a class of lure nonlinear systems," in *2019 IEEE International Conference on Automatic*

Control and Intelligent Systems (I2CACIS), pp. 179–184, Selangor, Malaysia, 2019.

[6] L. Negash, S. Kim, and H. Choi, "Distributed observes for cyberattack detection and isolation in formation-flying unmanned aerial vehicles," *Journal of Aerospace Information Systems*, vol. 14, no. 10, pp. 551–565, 2017.

[7] L. Yin, J. Liu, P. Yang, and J. Shi, "Sliding mode observer-based active fault tolerant control for UAVs formation," *IOP Conference Series: Materials Science and Engineering*, vol. 452, 2018.

[8] A. Cristofaro and T. A. Johansen, "An unknown input observer based control allocation scheme for icing diagnosis and accommodation in overactuated UAVs," in *2016 European Control Conference (ECC)*, pp. 2171–2178, Aalborg, Denmark, 2016.

[9] D. Rotondo, A. Cristofaro, T. Johansen, F. Nejjari, and V. Puig, "Diagnosis of icing and actuator faults in UAVs using LPV unknown input observers," *Journal of Intelligent & Robotic Systems*, vol. 91, no. 3-4, pp. 651–665, 2018.

[10] A. Abbaspour, P. Aboutalebi, K. K. Yen, and A. Sargolzaei, "Neural adaptive observer-based sensor and actuator fault detection in nonlinear systems: application in UAV," *ISA Transactions*, vol. 67, pp. 317–329, 2017.

[11] Y. Liang, Q. Dong, and Y. Zhao, "Adaptive leader-follower formation control for swarms of unmanned aerial vehicles with motion constraints and unknown disturbances," *Chinese Journal of Aeronautics*, vol. 33, no. 11, pp. 2972–2988, 2020.

[12] X. Wang, Y. Yu, and Z. Li, "Distributed sliding mode control for leader-follower formation flight of fixed-wing unmanned aerial vehicles subject to velocity constraints," *International Journal of Robust and Nonlinear Control*, vol. 31, no. 6, pp. 2110–2125, 2021.

[13] X. Liu, J. Han, and X. Wei, "Intermediate observer based distributed fault estimation for multi-agent systems," *Acta Automatica Sinica*, vol. 46, no. 1, pp. 142–152, 2020.

[14] B. Jiang, P. Shi, and K. Zhang, "Fast fault estimation and accommodation for dynamical systems," *IET Control Theory & Applications*, vol. 3, no. 2, pp. 189–199, 2009.

[15] K. Zhang, B. Jiang, and A. Shumsky, "A new criterion of fault estimation for neutral delay systems using adaptive observer," *Acta Automatica Sinica*, vol. 35, no. 1, pp. 85–91, 2009.

[16] J. Zhu, G. Yang, H. Wang, and F. Wang, "Fault estimation for a class of nonlinear systems based on intermediate estimator," *IEEE Transactions on Automatic Control*, vol. 61, no. 9, pp. 2518–2524, 2016.

[17] J. Zhu and G. Yang, "Robust distributed fault estimation for a network of dynamical systems," *IEEE Transactions on Control of Network Systems*, vol. 5, no. 1, pp. 14–22, 2018.

[18] J. Shen, X. Wang, Q. Liu, J. Yu, G. Chen, and X. Tian, "Analysis of time coordinated guidance control for leader-follower smart ammunition formation," in *2020 3rd International Conference on Unmanned Systems (ICUS)*, pp. 214–219, Harbin, China, 2020.

[19] J. Zhang, A. K. Swain, and S. K. Nguang, "Robust sensor fault estimation scheme for satellite attitude control systems," *Journal of the Franklin Institute*, vol. 350, no. 9, pp. 2581–2604, 2013.

[20] C. A. Rabbath and N. Léchevin, *Safety and Reliability in Cooperating Unmmaned Aerial Systems*, World Scientific Publishing Co. Pte. Ltd., Singapore, 2010.

[21] M. Guiatni, H. Saidani, and Y. Bouzid, "Fault tolerant control design for actuator loss of effectiveness in quadrotor Uavs," in *2019 International Russian Automation Conference (RusAutoCon)*, pp. 1–7, Sochi, Russia, 2019.

[22] M. I. Momtaz and A. Chatterjee, "Hierarchical state space checks for errors in sensors, actuators and control of nonlinear systems: diagnosis and compensation," in *2019 IEEE 28th Asian Test Symposium (ATS)*, pp. 141–1415, Kolkata, India, 2019.

[23] O. Prakash, A. K. Samantaray, and R. Bhattacharyya, "Model-based diagnosis of multiple faults in hybrid dynamical systems with dynamically updated parameters," *IEEE Transactions on Systems, Man, and Cybernetics: Systems*, vol. 49, no. 6, pp. 1053–1072, 2019.

[24] M. Qian, B. Jiang, and H. H. Liu, "Dynamic surface active fault tolerant control design for the attitude control systems of UAV with actuator fault," *International Journal of Control, Automation and Systems*, vol. 14, no. 3, pp. 723–732, 2016.

[25] Z. Yu, Y. Qu, and Y. Zhang, "Distributed fault-tolerant cooperative control for multi-UAVs under actuator fault and input saturation," *IEEE Transactions on Control Systems Technology*, vol. 27, no. 6, pp. 2417–2429, 2019.

[26] Y. Xiao, Y. Fu, C. Wu, and P. Shao, "Modified model reference adaptive control of UAV with wing damage," in *2016 2nd International Conference on Control, Automation and Robotics (ICCAR)*, pp. 189–193, Hong Kong, China, 2016.

[27] B. Fan, X. Zhang, B. Tian, and L. Guo, "Fault-tolerant control for unmanned aerial vehicle with wing damaged," in *IECON 2017-43rd Annual Conference of the IEEE Industrial Electronics Society*, pp. 3191–3196, Beijing, China, 2017.

[28] P. B. Sujit and J. B. Sousa, "Multi-UAV task allocation with communication faults," in *2012 American Control Conference (ACC)*, pp. 3724–3729, Montreal, QC, Canada, 2012.

[29] M. Labbadi and M. Cherkaoui, "Robust integral terminal sliding mode control for quadrotor UAV with external disturbances," *International Journal of Aerospace Engineering*, vol. 2019, Article ID 2016416, 10 pages, 2019.

[30] F. F. Khan, T. Samira, A. Jana, and K. N. E. Alam Siddiquee, "Performance of agro-sensors: Assessment of optimality in routing protocols of MANET in wireless sensor networks," in *2016 International Conference on Intelligent Control Power and Instrumentation (ICICPI)*, pp. 98–102, Kolkata, 2016.

[31] H. Kim and J. Ben-Othman, "A collision-free surveillance system using smart UAVs in multi domain IoT," *IEEE Communications Letters*, vol. 22, no. 12, pp. 2587–2590, 2018.

[32] J. Ghommam, L. F. Luque-Vega, and M. Saad, "Distance-based formation control for quadrotors with collision avoidance via Lyapunov barrier functions," *International Journal of Aerospace Engineering*, vol. 2020, Article ID 2069631, 17 pages, 2020.

[33] D. Wang, T. Fan, T. Han, and J. Pan, "A two-stage reinforcement learning approach for multi-UAV collision avoidance under imperfect sensing," *IEEE Robotics and Automation Letters*, vol. 5, no. 2, pp. 3098–3105, 2020.

[34] H. Tanner and D. Christodoulakis, "Decentralized cooperative control of heterogeneous vehicle groups," *Robotics and Autonomous Systems*, vol. 55, no. 11, pp. 811–823, 2007.

[35] G. Ducard and H. P. Geering, "Efficient nonlinear actuator fault detection and isolation system for unmanned aerial vehicles," *Journal of Guidance, Control, and Dynamics*, vol. 31, no. 1, pp. 225–237, 2008.

[36] X. Cheng, C. Dong, G. H. Chen, W. J. Wang, and H. P. Dai, "Communication and networking techniques for formation control in UAV ad hoc networks," *Computer Science*, vol. 45, no. 11, pp. 1–12, 2018.

[37] R. Abdallah, R. Kouta, C. Sarraf, J. Gaber, and M. Wack, "Fault tree analysis for the communication of a fleet formation flight of UAVs," in *2017 2nd International Conference on System Reliability and Safety (ICSRS)*, pp. 202–206, Milan, Italy, 2017.

[38] J. Longting, W. Ruixuan, Z. Qirui, and W. Dong, "Anti-collision control of UAVs based on swarm intelligence mechanism," *Acta Aeronautica et Astronautica Sinica*, vol. 41, article 724291, Supplement 2, 2020.

[39] M. Khalid, "Crosswise wind shear represented as a ramped velocity profile impacting a forward-moving aircraft," *International Journal of Aerospace Engineering*, vol. 2019, Article ID 7594737, 18 pages, 2019.